

Manuscript Number: JCLEPRO-D-19-07060R3

Title: Municipal solid waste incineration bottom ash as Alkali-Activated Cement precursor depending on particle size

Article Type: Original article

Keywords: Bottom Ash; Waste Management; Alkali Activated Cement; Cement precursor

Corresponding Author: Dr. Josep Maria Ma. Chimenos, Ph.D.

Corresponding Author's Institution: University of Barcelona

First Author: Àlex Maldonado-Alameda

Order of Authors: Àlex Maldonado-Alameda; Jessica Giro-Paloma; Adela Svobodova-Sedlackova; Joan Formosa; Josep Maria Ma. Chimenos, Ph.D.

Abstract: Bottom Ash (BA) is the main by-product of municipal solid waste incineration (MSWI). It is stabilised outdoors to obtain weathered bottom ash (WBA) whose main application is in the construction sector as a secondary aggregate for road sub-base. Here, the aim of this work is to advance the study of the potential use of WBA as a precursor in the synthesis of new alkali-activated cements (AACs). An exhaustive physicochemical characterisation (X-ray fluorescence, X-ray diffraction, Fourier-transform infrared spectroscopy, inductively coupled plasma - optical emission spectroscopy, and Inductively coupled plasma - mass spectroscopy) of WBA was provided depending on its particle size (<30, 30-16, 16-8, 8-4, 4-2 and 2-0 mm). The study reveals that WBA is composed mainly of the essential reactive phases to form AACs, which are SiO<sub>2</sub>, Al<sub>2</sub>O<sub>3</sub>, and CaO. It is demonstrated the larger the particle size, the higher the content of SiO<sub>2</sub>; and the smaller the particle size, the higher the heavy metal(loid) content. The availability of reactive phases was analysed through chemical attacks with HF and NaOH solutions of different concentrations (2M, 4M, and 8M). The results demonstrate the availability of reactive phases (including 150 to 250 g·kg<sup>-1</sup> of SiO<sub>2</sub> and 50 to 65 g·kg<sup>-1</sup> of Al<sub>2</sub>O<sub>3</sub>) in all the particle size fractions studied. WBA potential will be of considerable use to formulate AACs, depending on the particle size fraction and the Si/Al ratio, both as the sole precursor and mixed with others.

**Title: Municipal solid waste incineration bottom ash as Alkali-Activated  
Cement precursor depending on particle size**

**Authors: A. Maldonado-Alameda, J. Giro-Paloma, A. Svobodova-Sedlackova,  
J. Formosa, J.M. Chimenos**

The responses to editor suggestions are presented below. Hopefully, we answered all the questions and clarified all issues. Enclosed, please find the revised manuscript.

**Answers to the Editor suggestions**

Is it possible to remove 'as a function of particle size in the title? It will look better and looks like a title rather than a sentence.

Thank you for the suggestion. The authors think that the part 'as a function of particle size' provide relevant information for the potential readers. However, the title has been modified to looks like a title.

Please remove those redundant words, e.g. Additionally, etc.

The redundant words were removed.

Please make the Conclusions more concise, of about 1-2 paragraph to only underscore the key results and how it contributes to the future work.

The conclusions have been changed. Now, they are more concise underscore the key results and to emphasise the future work.

# Municipal solid waste incineration bottom ash as Alkali-Activated Cement precursor depending on particle size

A. Maldonado-Alameda <sup>a</sup>, J. Giro-Paloma <sup>a</sup>, A. Svobodova-Sedlackova <sup>a</sup>, J. Formosa <sup>a</sup>,

J.M. Chimenos <sup>a,\*</sup>

<sup>a</sup> Departament de Ciència de Materials i Química Física, Universitat de Barcelona, C/ Martí i Franquès, 1, 08028, Barcelona, Spain.

\*Corresponding author e-mail: [chimenos@ub.edu](mailto:chimenos@ub.edu)

## Highlights

- Weathered bottom ash (WBA) potential as alkali-activation material has been evaluated.
- $\text{SiO}_2$ ,  $\text{Al}_2\text{O}_3$ , and  $\text{CaO}$  are the main components of WBA.
- The availability of  $\text{SiO}_2$  and  $\text{Al}_2\text{O}_3$  is high in the coarser fractions of WBA.
- After  $\text{NaOH}$  8M chemical attack, metal(loid)s content is high in the finest fractions.

1  
2  
3  
4  
5  
6  
7  
8  
9  
10  
11  
12  
13  
14  
15  
16  
17  
18  
19  
20  
21  
22  
23  
24  
25  
26  
27  
28  
29  
30  
31  
32  
33  
34  
35  
36  
37  
38  
39  
40  
41  
42  
43  
44  
45  
46  
47  
48  
49  
50  
51  
52  
53  
54  
55  
56  
57  
58  
59  
60  
61  
62  
63  
64  
65

# Municipal solid waste incineration bottom ash as Alkali-Activated Cement precursor depending on particle size

A. Maldonado-Alameda <sup>a</sup>, J. Giro-Paloma <sup>a</sup>, A. Svobodova-Sedlackova <sup>a</sup>, J. Formosa <sup>a</sup>,  
J.M. Chimenos <sup>a,\*</sup>

<sup>a</sup> Departament de Ciència de Materials i Química Física, Universitat de Barcelona, C/ Martí i Franquès, 1, 08028, Barcelona, Spain.

\*Corresponding author e-mail: [chimenos@ub.edu](mailto:chimenos@ub.edu)

## Abstract

1  
2 Bottom Ash (BA) is the main by-product of municipal solid waste incineration (MSWI). It is  
3  
4 stabilised outdoors to obtain weathered bottom ash (WBA) whose main application is in the  
5  
6 construction sector as a secondary aggregate for road sub-base. Here, the aim of this work is  
7  
8 to advance the study of the potential use of WBA as a precursor in the synthesis of new alkali-  
9  
10 activated cements (AACs). An exhaustive physicochemical characterisation (X-ray  
11  
12 fluorescence, X-ray diffraction, Fourier-transform infrared spectroscopy, inductively coupled  
13  
14 plasma – optical emission spectroscopy, and Inductively coupled plasma – mass  
15  
16 spectroscopy) of WBA was provided depending on its particle size (<30, 30-16, 16-8, 8-4, 4-2  
17  
18 and 2-0 mm). The study reveals that WBA is composed mainly of the essential reactive  
19  
20 phases to form AACs, which are SiO<sub>2</sub>, Al<sub>2</sub>O<sub>3</sub>, and CaO. It is demonstrated the larger the  
21  
22 particle size, the higher the content of SiO<sub>2</sub>; and the smaller the particle size, the higher the  
23  
24 heavy metal(loid) content. The availability of reactive phases was analysed through chemical  
25  
26 attacks with HF and NaOH solutions of different concentrations (2M, 4M, and 8M). The  
27  
28 results demonstrate the availability of reactive phases (including 150 to 250 g·kg<sup>-1</sup> of SiO<sub>2</sub>  
29  
30 and 50 to 65 g·kg<sup>-1</sup> of Al<sub>2</sub>O<sub>3</sub>) in all the particle size fractions studied. WBA potential will be  
31  
32 of considerable use to formulate AACs, depending on the particle size fraction and the Si/Al  
33  
34 ratio, both as the sole precursor and mixed with others.  
35  
36  
37  
38  
39  
40  
41  
42  
43  
44  
45

46 *Keywords:* Bottom Ash, Waste Management, Alkali Activated Cement, Cement precursor  
47  
48  
49  
50  
51  
52  
53  
54  
55  
56  
57  
58  
59  
60  
61  
62  
63  
64  
65

1  
2  
3  
4  
5 **1. Introduction**  
6

7 The Waste Framework Directive (European Parliament and Council, 2008) of the  
8 European Parliament and the policies of the member states of the European Union (EU) focus  
9 on maintaining the value of products, materials and resources for as long as possible, moving  
10 towards a circular economy (European Commission, 2017). The priority of the member states  
11 is to continue promoting and developing systems and infrastructures that provide proper  
12 municipal solid waste (MSW) management. According to the EU waste management  
13 hierarchy (European Parliament and Council, 2008), landfilling is the least preferable option,  
14 and its use is expected to be limited to as little as 10% by the year 2030 (European  
15 Commission, 2015). The EU order of priority establishes prevention, reuse, and recycling as  
16 the main processes in MSW management. However, one of the most suitable alternatives to  
17 landfilling for MSW is energy recovery in waste-to-energy (WtE) plants, which contribute to  
18 reducing the volume (up to 90%) and weight (up to 75%) of municipal waste (MW) (Cheng  
19 and Hu, 2010).  
20  
21  
22  
23  
24  
25  
26  
27  
28  
29  
30  
31  
32  
33  
34  
35  
36  
37

38 Incineration bottom ash (IBA) is the main by-product of the combustion process in WtE  
39 plants (Chimenos et al., 1999). Around  $18 \text{ Mt}\cdot\text{y}^{-1}$  of IBA is produced in the EU (CEWEP,  
40 2016). This MSW incineration (MSWI) residue, which is approximately 85% of the solid  
41 resulting from combustion, can be considered as slag, granular material, and non-hazardous  
42 waste (Valle-zermeño et al., 2017). IBA is mainly composed of silicon, calcium, iron,  
43 aluminium, and sodium, although it also contains small amounts of several heavy  
44 metal(loid)s. For its subsequent reuse as a secondary material, a weathering (aging) process  
45 lasting 2-3 months is necessary, during which the IBA is stored outdoors. This procedure  
46 results in carbonation and oxidation of the IBA and its consequent pH stabilisation with  
47  
48  
49  
50  
51  
52  
53  
54  
55  
56  
57  
58  
59  
60  
61  
62  
63  
64  
65

1 values between 8 to 10, as well as the neo-formation and hydration of mineral phases, among  
2 other consequences (Chimenos et al., 2000). The material resulting from the weathering  
3 process is known as weathered bottom ash (WBA). Approximately 85% of WBA is glass,  
4 ceramics, stone, brick, concrete, ash, and melting products, which has a grain size distribution  
5 and technical properties that are similar to those of natural sand and gravel (Zhang and  
6 Shimaoka, 2013). The potential applications of the WBA are plenty and assorted. In many  
7 countries like France, Italy, the Netherlands or China, there is a great interest in valorising  
8 WBA. During the last years several studies have been carried out in some sectors. In the field  
9 of civil engineering as secondary aggregate for road construction (Cioffi et al., 2011; Hjelmar  
10 et al., 2007), embankments (Pecqueur et al., 2001), and pavements (Toraldó et al., 2013), as  
11 well as concrete filling (Ginés et al., 2009). Regarding the building sector it is studied its  
12 application as ceramic material such as tiles, bricks and glass-ceramics (Lancellotti et al.,  
13 2014). In the chemical engineering field, studies have been carried out for its use as an  
14 absorbent for wastewater treatment processes (Shim et al., 2003) as well as co-disposal and  
15 biogas production (Silva et al., 2017).

16 Besides the concerns regarding waste management, the cement industry can also present a  
17 threat to the environment (Aljerf, 2015). Cement production is responsible for some 5%-7%  
18 of CO<sub>2</sub> emissions worldwide (McLellan et al., 2011) and it is estimated to consume 2% of  
19 global primary energy (Chen, 2009). The cement industry must face the challenge of finding  
20 new processes to manufacture in a more ecological and respectful way, reducing energy  
21 consumption and greenhouse gas emissions. The use of by-products such as WBA to  
22 manufacture cementitious materials could be one way to obtain eco-friendly cements. Full-  
23 scale demonstrations of the technical feasibility of unbound and cement-bound sub-base  
24 layers containing WBA, i.e. general ceramics, glass or glass-ceramics, have been successful  
25 (Arm, 2003; Magnusson, 2005). Alkali-activated cements (AACs) have become an ideal

1 alternative to ordinary Portland cement (OPC) because of their properties. AACs have good  
2 compression strength (Alonso et al., 2000), high resistance to chemical attack by aggressive  
3 aqueous and acid solutions (Bakharev, 2005), and resistance to fire and high temperature  
4 (Murri et al., 2013). However, the main benefit exhibited by AACs is their greater respect for  
5 the environment, compared to other cementitious materials. If AACs are compared to OPC,  
6 the former reduces the CO<sub>2</sub> emissions and the energy consumption associated with cement  
7 manufacture (Van Deventer et al., 2012). It is important to highlight that AACs, as most of  
8 the new cements produced using industrial by-products or waste (Bernal et al., 2016), follow  
9 the zero waste principle (Komnitsas, 2011). For this reason, AACs are considered new  
10 sustainable and eco-friendly cements (Phair, 2006). The alkaline activation reaction is a  
11 polycondensation which starts when a solid powder precursor (based on alumino-silicates) is  
12 dissolved in an alkaline medium. This reaction generates free silica tetrahedral and aluminium  
13 cations coordinated with oxygen, which will form a 3D structure (Duxson et al., 2007; Singh  
14 et al., 2015). The final AACs properties depend on the precursor, the relation between the  
15 proportions of SiO<sub>2</sub> and Al<sub>2</sub>O<sub>3</sub>, the CaO content, the alkali activator used, and the curing  
16 temperature (Aljerf, 2015).

17  
18  
19  
20  
21  
22  
23  
24  
25  
26  
27  
28  
29  
30  
31  
32  
33  
34  
35  
36  
37  
38  
39 Previous studies have revealed that WBA is mainly composed of SiO<sub>2</sub>, Al<sub>2</sub>O<sub>3</sub>, and CaO  
40 (Valle-zermeño et al., 2017; Wei et al., 2011), which are the essential mineral phases required  
41 to formulate AACs. WBA contains enough glassy materials (primary or secondary glass)  
42 (Valle-zermeño et al., 2017), as well as important amounts of both sources of aluminium and  
43 calcium for its use as a precursor in the formulation of AACs. However, WBA presents a high  
44 heterogeneity and its composition varies depending on particle size fraction (Valle-zermeño et  
45 al., 2017). The availability of reactive phases (SiO<sub>2</sub> and Al<sub>2</sub>O<sub>3</sub>) in each fraction will vary as a  
46 function of the composition and the alkali activator concentration. Physicochemical  
47 characterisation and determination of SiO<sub>2</sub> and Al<sub>2</sub>O<sub>3</sub> availability will allow to determine the  
48  
49  
50  
51  
52  
53  
54  
55  
56  
57  
58  
59  
60  
61  
62  
63  
64  
65

possibilities of using a specific WBA particle size as the sole precursor in the synthesis of AACs; or whether, additional sources (precursors) would be required to achieve an optimal SiO<sub>2</sub>/Al<sub>2</sub>O<sub>3</sub> ratio.(Aljerf, 2015).

In this research, the main goal is to determine the added value of WBA as precursor in AACs formulation to contribute to the EU's objectives in the waste management and valorisation fields. This work focuses on the determination of SiO<sub>2</sub> and Al<sub>2</sub>O<sub>3</sub> available in WBA, as the reactive phases required to formulate new AACs, as a function of WBA particle size. The availability of these reactive phases in each fraction is analysed through chemical attacks, and it is related to the amorphous phases content, as well as with the material characterisation determined elsewhere (Chimenos et al., 1999; Valle-zermeño et al., 2017). For each particle size fraction of WBA under study, it is analysed the concentration of heavy metals and metal(loid)s leached during the alkaline activation of reactive phases to determine the potential release of WBA used as a precursor in the formulation of AACs.

## 2. Experimental procedure

### 2.1. Materials

The WBA sample was supplied by the company Valorización de Escorias para la Construcción S.A. (VECSA), which is responsible for valorising and commercialising the IBA collected from the WtE plant located in Tarragona (Spain). The feed stream treated in the incineration plant (140 kt·y<sup>-1</sup>) is mainly composed of household rubbish with a small input from commercial sources. The incineration temperature is around 950°C (Chimenos et al., 1999). Approximately, 32 kt·y<sup>-1</sup> of fresh IBA is produced by the incineration plant annually and treated to recover both ferrous and non-ferrous metals, as well as the lightweight materials that can be removed. After being conditioned, the resultant IBA is stockpiled outdoors for at least three months, to ensure immobilisation of heavy metal(loid)s by weathering and to obtain WBA. Due to the heterogeneity of IBA, for this study around 100 kg

of WBA was collected from various stockpiles, homogenised, and stored in a 30 L plastic container.

2.2. Samples preparation

The samples preparation scheme is shown in Fig. 1. First, the WBA was dried overnight at 105°C in a stove. Then, the particle size distribution (PSD) was analysed by sieving the dried WBA through openings standards of 2, 4, 8 and 16 mm (Valle-zermeño et al., 2017). After sieving, around 100 g of each fraction (<30, 30-16, 16-8, 8-4, 4-2 and 2-0 mm) was initially quartered and crushed in a jaw crusher. The samples were milled in a vibratory disc mill, using a grinding set made of hardened steel. It is important to highlight that the <30 mm fraction corresponds to the bulk sample without being sieved. The milling continued until the whole sample passed through a sieve of 80 µm mesh (except for the ferrous and non-ferrous metal particles which, due to their ductility, were retained in the sieves) resulting in a homogeneous powder. A magnet (Nd; 0.485 T) was passed over the sample to remove magnetic particles.

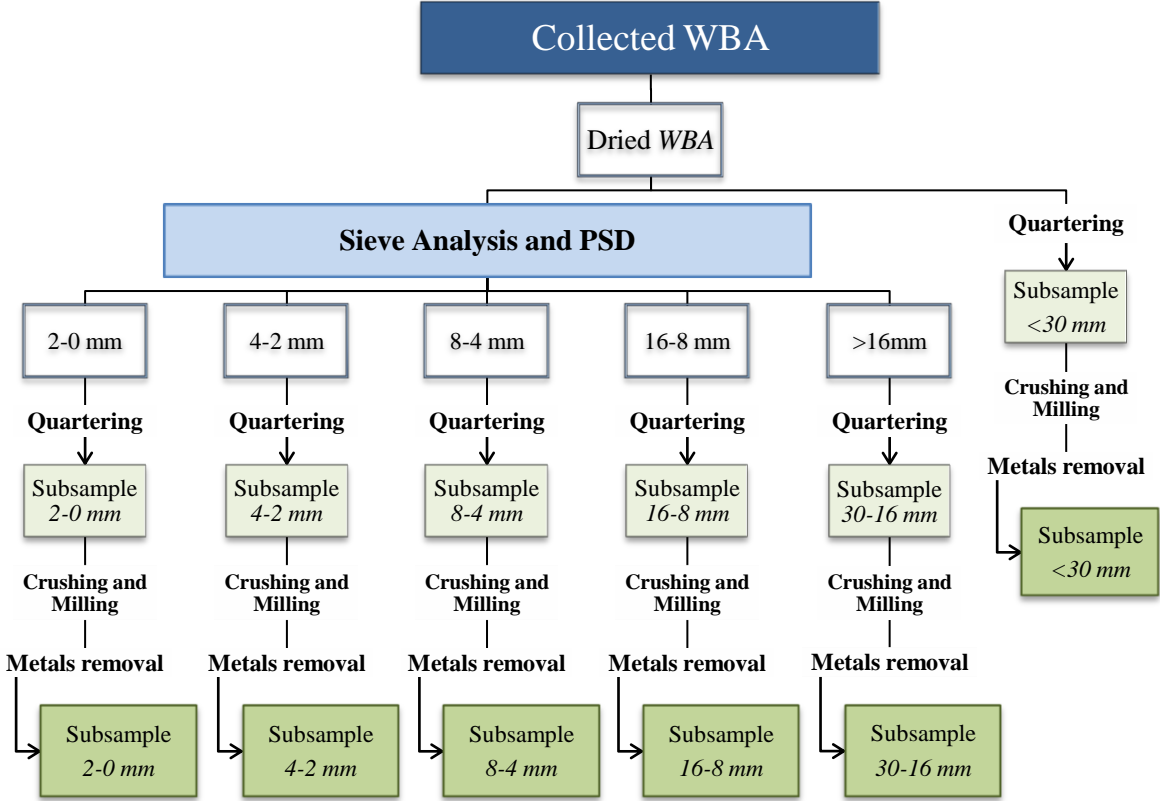


## Fig. 1. Scheme of the preparation of samples.

### 2.2. WBA Characterization

#### 2.2.1. Physicochemical characterization

For each powdered size fraction of the WBA, the chemical composition of the major and minor elements was determined by means of X-ray fluorescence spectroscopy (XRF) using a Panalytical Philips PW 2400 sequential X-ray spectrometer with UniQuant<sup>®</sup> V5.0 software.

The mineral and crystalline phases of the powdered WBA fractions were identified by X-ray diffraction analysis (XRD) using a Bragg–Brentano Siemens D-500 powder diffractometer with CuK $\alpha$  radiation. The amorphous index for samples containing both amorphous and crystalline phases was quantified with the external standard method (Jansen et al., 2011; Snellings et al., 2014).

#### 2.2.2. SiO<sub>2</sub> and Al<sub>2</sub>O<sub>3</sub> availability

The availability of reactive phases (SiO<sub>2</sub> and Al<sub>2</sub>O<sub>3</sub>) was determined through chemical attacks with HF (1% v/v) and NaOH solutions (2M, 4M, and 8M) (Aljerf, 2015; Ruiz-Santaquiteria et al., 2011). For these experimental trials, one gram of WBA sample was mixed with 100 mL of each activating solution and stirred constantly for 5 h in a sealed plastic container, at 80°C for alkaline solutions, or at room temperature in the case of HF. The resulting solution was filtered and analysed by means of inductively coupled plasma optical emission spectrometry (ICP-OES) using Perkin Elmer Optima ICP-OES 3200 RL equipment to quantify the Si and Al leached (Ruiz-Santaquiteria et al., 2011). It was used Fourier-transform infrared spectroscopy by attenuated total reflection (FT-IR ATR) to evaluate the chemical structure and composition and compared both the initial and attacked WBA powders (with HF and the different NaOH solutions) using Spectrum Two<sup>™</sup> equipment from Perkin Elmer.

#### 2.2.3. Heavy metals content

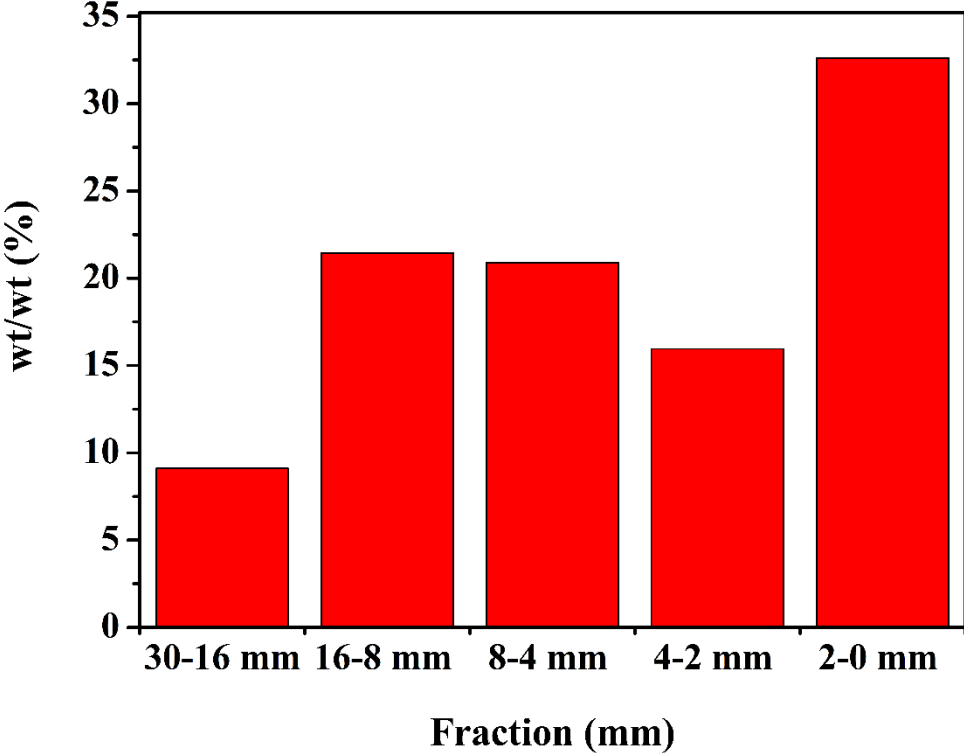
1 The potential environmental impact of the WBA was assessed by analysing the heavy  
2 metal(loid)s released in the filtered NaOH 8M solutions during the alkaline activation using a  
3 Perkin Elmer ELAN 6000 ICP mass spectrometry (ICP-MS) device.  
4  
5

6  
7 **3. Results and discussion**  
8

9  
10 *3.1. WBA Characterization*

11  
12 *3.1.1. Physicochemical characterization*

13  
14 Fig. 2 shows the PSD of the WBA. Around 50% of the WBA corresponds to fractions  
15 below 4 mm (fine fraction), in agreement with previous findings (Chimenos et al., 1999;  
16 Valle-zermeño et al., 2017).  
17  
18  
19  
20  
21  
22  
23



24  
25  
26  
27  
28  
29  
30  
31  
32  
33  
34  
35  
36  
37  
38  
39  
40  
41  
42  
43  
44  
45  
46  
47  
48  
49  
50  
51 **Fig. 2. Particle Size Distribution of Weathered Bottom Ash**

52 The major and minor elemental composition, as elemental oxides and trace-elements in  
53 each size fraction of WBA analysed, are given in Table 1. As expected, the most abundant  
54 oxides were SiO<sub>2</sub>, CaO, and Al<sub>2</sub>O<sub>3</sub>, which are the key compounds in cementitious materials  
55  
56  
57  
58  
59  
60  
61  
62  
63  
64  
65

(Aljerf, 2015; Roy, 1999). As can be seen, the contents of these oxides varied, depending on the size fraction. The highest SiO<sub>2</sub> content was in coarse fractions (30-16, 16-8, and 8-4 mm) due to the primary and secondary glass present, as well as the synthetic ceramic materials present in these fractions (Chimenos et al., 2003; Valle-zermeño et al., 2017). As for Al<sub>2</sub>O<sub>3</sub>, its content trends to increase as the particle size decreases, except for the 30-16 mm fraction. This is due to the Eddy current device, because only recovers the non-ferrous fraction from the particle size fractions greater 10 mm. Moreover, the 30-16 mm size fraction contains a large amount of synthetic ceramics (Valle-zermeño et al., 2017). The high content of CaO in the finest fractions (4-2 and 2-0 mm) is due to the presence of large amounts of calcium carbonates that are neo-formed during the weathering process of portlandite (Chimenos et al., 2003). This CaO high amount is also because of the presence of cementitious materials, based on OPC, and synthetic ceramics from small domestic works. These materials are fragmented by mechanical attrition and thermal shock inside the combustion furnaces (Aljerf, 2015). It is important to note that the major and minor element contents of the <30 mm fraction agree with the contents calculated from the XRF results and the PSD weighting for each fraction (Fig. 2).

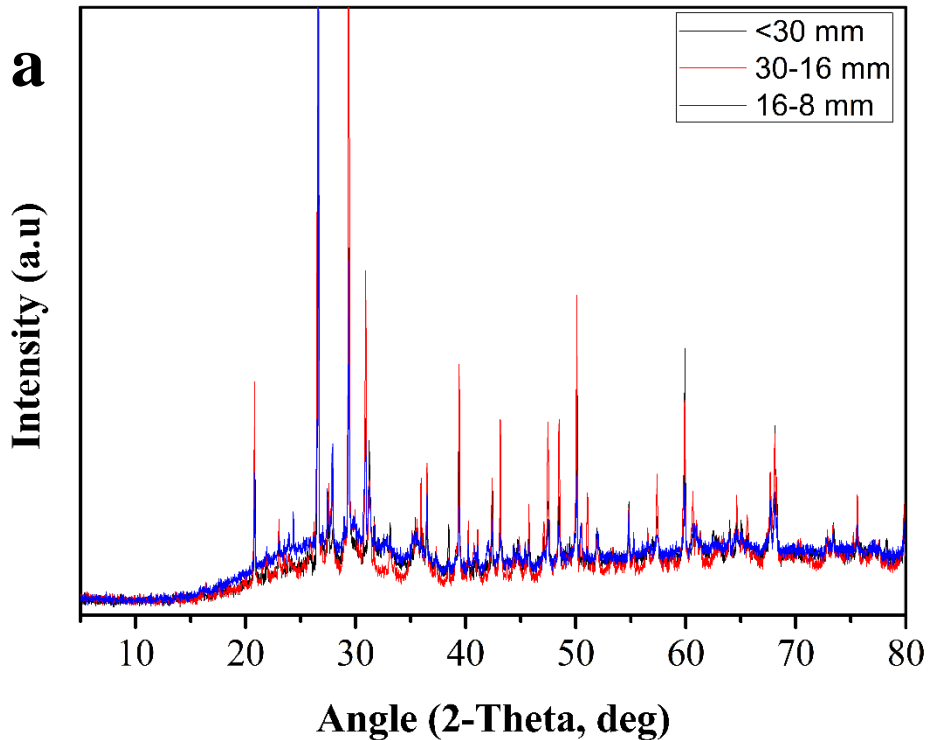
**Table 1. Major-, minor- and trace-elements for each size fraction of WBA.**

	(wt. %)					
	2-0 mm	4-2 mm	8-4 mm	16-8 mm	30-16 mm	<30 mm
<b>SiO<sub>2</sub></b>	25.11	39.02	54.45	59.3	50.23	45.44
<b>CaO</b>	23.77	19.35	15.15	13.6	16.25	17.55
<b>Al<sub>2</sub>O<sub>3</sub></b>	11.19	9.62	7.32	6.74	12.39	10.38
<b>Na<sub>2</sub>O</b>	2.78	4.93	8.14	7.77	3.11	5.04
<b>K<sub>2</sub>O</b>	1.11	1.41	1.25	1.61	1.95	1.54
<b>Fe<sub>2</sub>O<sub>3</sub></b>	7.22	6.89	5.43	4.19	3.49	6.08
<b>MgO</b>	2.88	3.24	1.99	2.30	2.74	2.66
<b>TiO<sub>2</sub></b>	0.82	0.67	0.44	0.37	0.56	0.65
<b>Cl<sup>-</sup></b>	1.99	1.14	0.62	0.40	0.93	1.42
<b>SO<sub>3</sub></b>	3.57	1.59	0.96	0.63	2.27	2.57
<b>Mn</b>	0.05	0.03	0.03	0.02	0.02	0.03
<b>Cu</b>	0.18	0.13	0.10	0.04	0.04	0.13
<b>Zn</b>	0.73	0.39	0.64	0.09	0.18	0.51
<b>Br</b>	< 0.01	< 0.01	< 0.01	< 0.01	< 0.01	< 0.01

	<b>Rb</b>	< 0.01	0.01	< 0.01	0.01	0.01	< 0.01
1	<b>Sr</b>	0.08	0.08	0.04	0.06	0.04	0.07
2	<b>Y</b>	< 0.01	< 0.01	< 0.01	n.d.	< 0.01	< 0.01
3	<b>Zr</b>	0.03	0.03	0.04	0.11	0.12	0.03
4	<b>Nb</b>	< 0.01	< 0.01	< 0.01	n.d.	< 0.01	< 0.01
5	<b>Sn</b>	0.03	0.02	0.01	0.01	0.02	0.02
6	<b>Sb</b>	0.02	0.01	0.01	< 0.01	0.01	0.01
7	<b>Ba</b>	0.15	0.10	0.07	0.04	0.05	0.07
8	<b>Pb</b>	0.15	0.34	0.13	0.05	0.04	0.11
9							
10	<b>LOI</b>	18.13	10.98	3.17	2.65	5.54	5.78

\*Loss on ignition at 1,000 °C.

The XRD patterns of the <30, 30-16, 16-8 mm fractions shown in Fig. 3a demonstrates that the WBA is a heterogeneous material (Giro-Paloma et al., 2017b), which has low crystallinity and is mainly composed of amorphous phases, as shown between the angular range from 20° to 35° (2 $\theta$ ). The Fig. 3b shows the dominant peaks in XRD patterns. The only crystalline phases present in all the fractions were quartz and calcite.



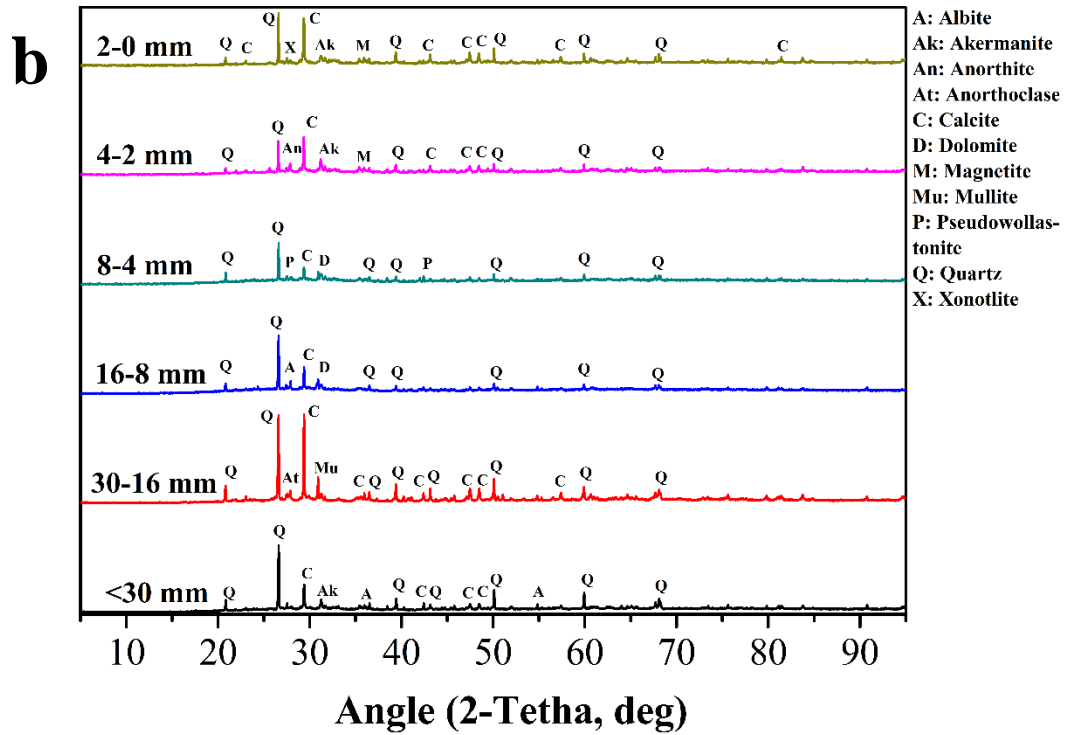


**Fig. 3. (a) XRD patterns of <30, 30-16, and 16-8 mm fractions (b) Dominant peaks of XRD patterns of all samples**

The main crystalline phases determined, depending on the size fraction, are shown in Table 2. The mineralogical compositions are similar, being the phases rich in Si, Al and Ca (quartz, calcite, albite, dolomite, etc.) more abundant. It is important to highlight the presence of metallic phases in the finest fractions (<30, 4-2 and 2-0 mm) and the great variety of silico-aluminate phases in all the fractions while being more abundant in coarse fractions.

**Table 2. Major crystalline phases in WBA samples.**

Mineral Phase	Fraction					
	2-0 mm	4-2 mm	8-4 mm	16-8 mm	30-16 mm	<30 mm
Albite (NaAlSi <sub>3</sub> O <sub>8</sub> )			✓	✓	✓	✓
Akermanite (Ca <sub>2</sub> MgSi <sub>2</sub> O <sub>7</sub> )	✓	✓	✓		✓	✓
Aluminium (Al)			✓			✓
Anorthite (CaAl <sub>2</sub> Si <sub>2</sub> O <sub>8</sub> )		✓				
Anorthoclase					✓	

1	((Na,K)AlSi <sub>3</sub> O <sub>8</sub> )						
2	Calcite	✓	✓	✓	✓	✓	✓
3	(CaCO <sub>3</sub> )						
4	Cesante	✓					
5	(Ca <sub>2</sub> Na <sub>3</sub> [(OH)(SO <sub>4</sub> ) <sub>3</sub> ])						
6	Cristobalite (SiO <sub>2</sub> )	✓	✓				✓
7							
8	Diopside (CaMgSi <sub>2</sub> O <sub>6</sub> )				✓		
9							
10	Dolomite			✓	✓	✓	
11	(CaMg(CO <sub>3</sub> ) <sub>2</sub> )						
12	Hematite (Fe <sub>2</sub> O <sub>3</sub> )	✓					✓
13							
14	Magnetite (Fe <sub>3</sub> O <sub>4</sub> )	✓	✓				✓
15	Mullite (Al <sub>6</sub> Si <sub>2</sub> O <sub>13</sub> ),					✓	
16	Pseudowollastonite			✓			
17	(Ca <sub>3</sub> Si <sub>3</sub> O <sub>9</sub> ),						
18	Quartz (SiO <sub>2</sub> )	✓	✓	✓	✓	✓	✓
19							
20	Wustite (FeO)			✓			
21							
22	Xonotlite	✓					
23	(Ca <sub>6</sub> Si <sub>6</sub> O <sub>17</sub> (OH) <sub>2</sub> )						

From the XRD patterns of each size fraction, the amorphous phases of the samples were quantified (Jansen et al., 2011; Snellings et al., 2014). Due to their abundance, quartz and amorphous glass samples were used as external patterns for this quantification. First, the crystalline compound was determined and then the amorphous phases were derived by differences, in the main angular range from 5° to 80° (2θ). The results are shown in Table 3, where the amorphous index of the particle size fractions was 44%-70%. As expected, the 30-16, 4-2, and 2-0 mm size fractions presented the lowest amorphous index because of their high content in synthetic ceramics and metal compounds, in contrast to the rest of the fractions where the amorphous amount is around or above 60%. It is important to highlight that the amorphous index of the <30 mm is in agreement with that calculated using the external standard method and the PSD weighting of each fraction (Fig. 2).

Table 3. Amorphous content (wt.%) in the size fractions of WBA.

Size Fractions	Amorphous content (wt.%)
<30 mm	60
30-16 mm	44

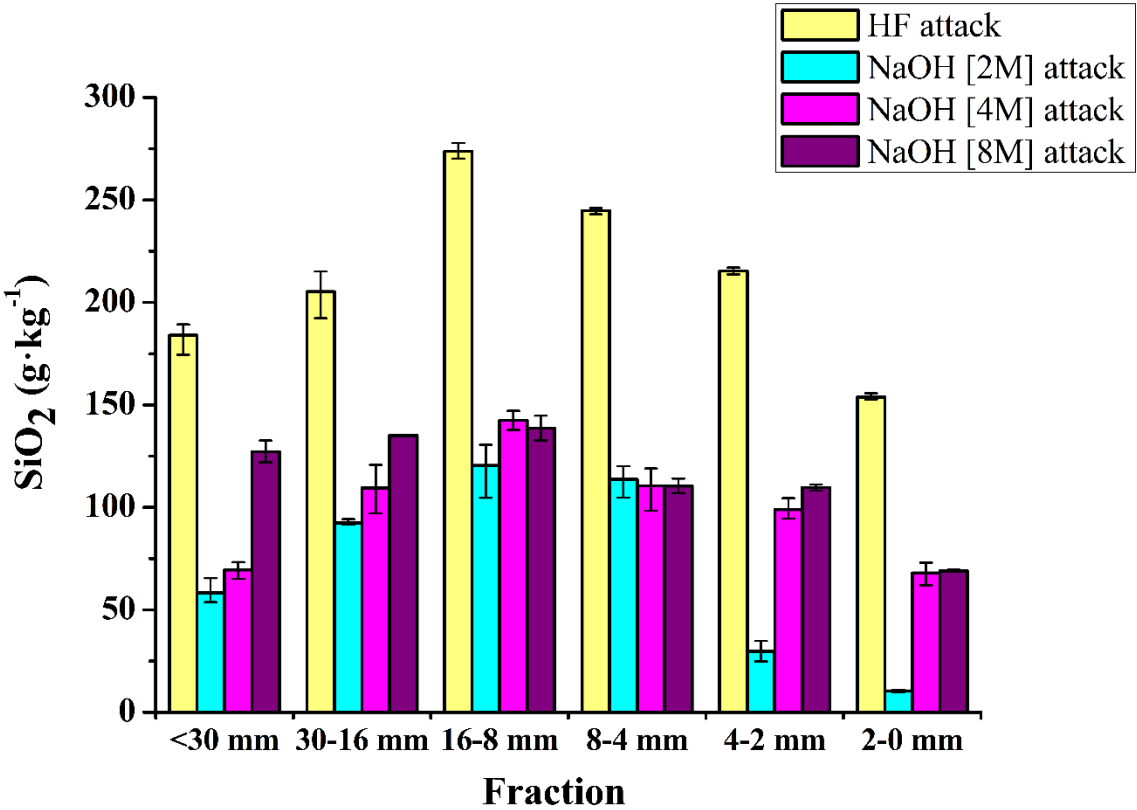
<b>16-8 mm</b>	66
<b>8-4 mm</b>	70
<b>4-2 mm</b>	53
<b>2-0 mm</b>	49

### 3.1.2. *SiO<sub>2</sub> and Al<sub>2</sub>O<sub>3</sub> availability*

XRF and XRD results show a large content of silico-aluminate phases and amorphous phases, but not all of these are available to react with the activating solution and form AACs. In fact, although thermodynamics allows certain reaction mechanisms, the chemical kinetics shows that some of these require very long reaction times that cannot be assumed. It is known that the crystalline phases are far less reactive than the amorphous phases, and that the active surface of the particles and their size. The reaction temperature and the concentration of the activators, are some of the important parameters for activation of the reactive phases (Ruiz-Santaquiteria et al., 2011). Accordingly, for each WBA particle size fraction, a chemical attack test was performed to determine the real amount ( $\text{g}\cdot\text{kg}^{-1}$  of WBA) of  $\text{SiO}_2$  and  $\text{Al}_2\text{O}_3$  available to form AACs. It is expected that most of the  $\text{SiO}_2$  and  $\text{Al}_2\text{O}_3$  available come from the amorphous phases. To a greater or lesser extent, all the particle size fractions contain  $\text{SiO}_2$  and  $\text{Al}_2\text{O}_3$  amorphous phases, as shown in Figs. 4 to 6.

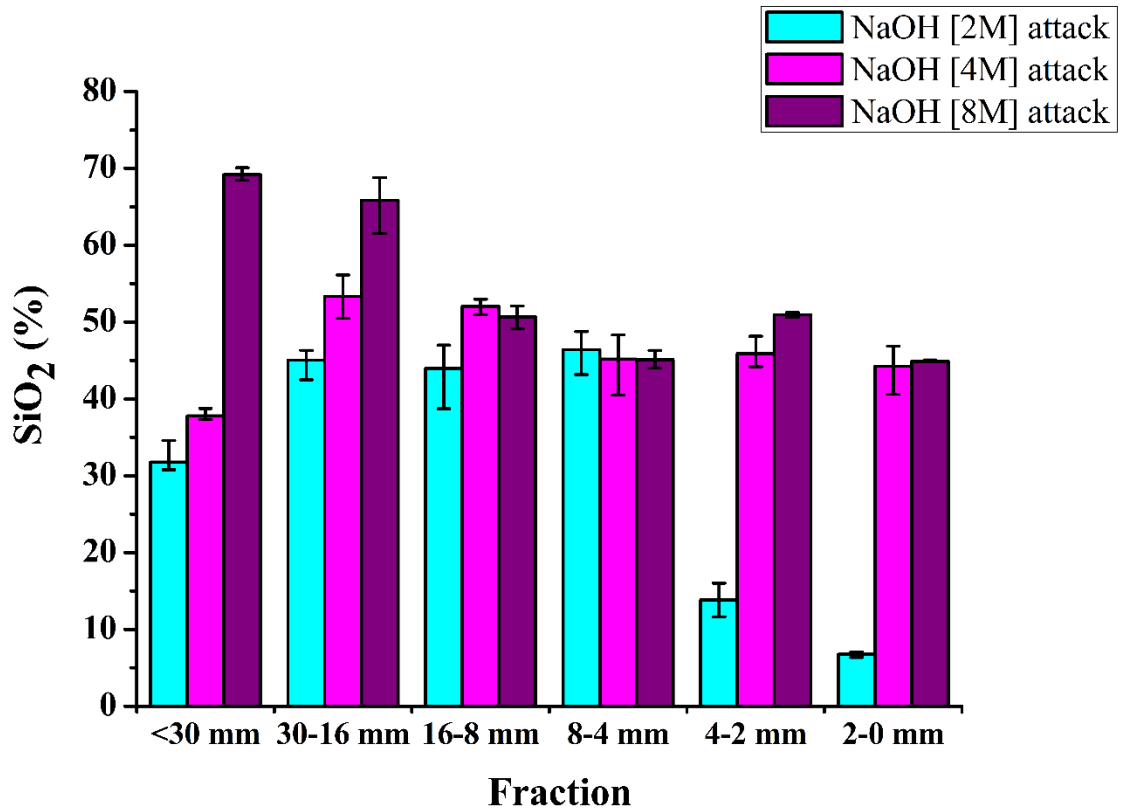
Focusing on the NaOH chemical attacks as a function of WBA particle size fraction, Fig. 4 shows that there is a broad trend (except for 8-4 and 16-8 mm) to increase  $\text{SiO}_2$  availability as the NaOH concentration increases. This tendency is due to the highly aggressive chemical attack (from 2M to 8M). Moreover, if it is compared the trend for all the fractions as a function of chemical attack, the same curve results in all cases and the maximum value was for the 16-8 mm fraction. Analysing the  $\text{SiO}_2$  availability of each fraction with the primary and secondary glass results obtained in a previous study (Valle-zermeño et al., 2017), validates this trend, except for the results in the 30-16 mm fraction. In this last case, the  $\text{SiO}_2$  extracted with chemical attacks comes from the synthetic ceramics. It is important to highlight

that the HF attack indicated the existence of a large amount of available SiO<sub>2</sub> amorphous phases that were not extracted with the NaOH chemical attacks, since they are less aggressive.



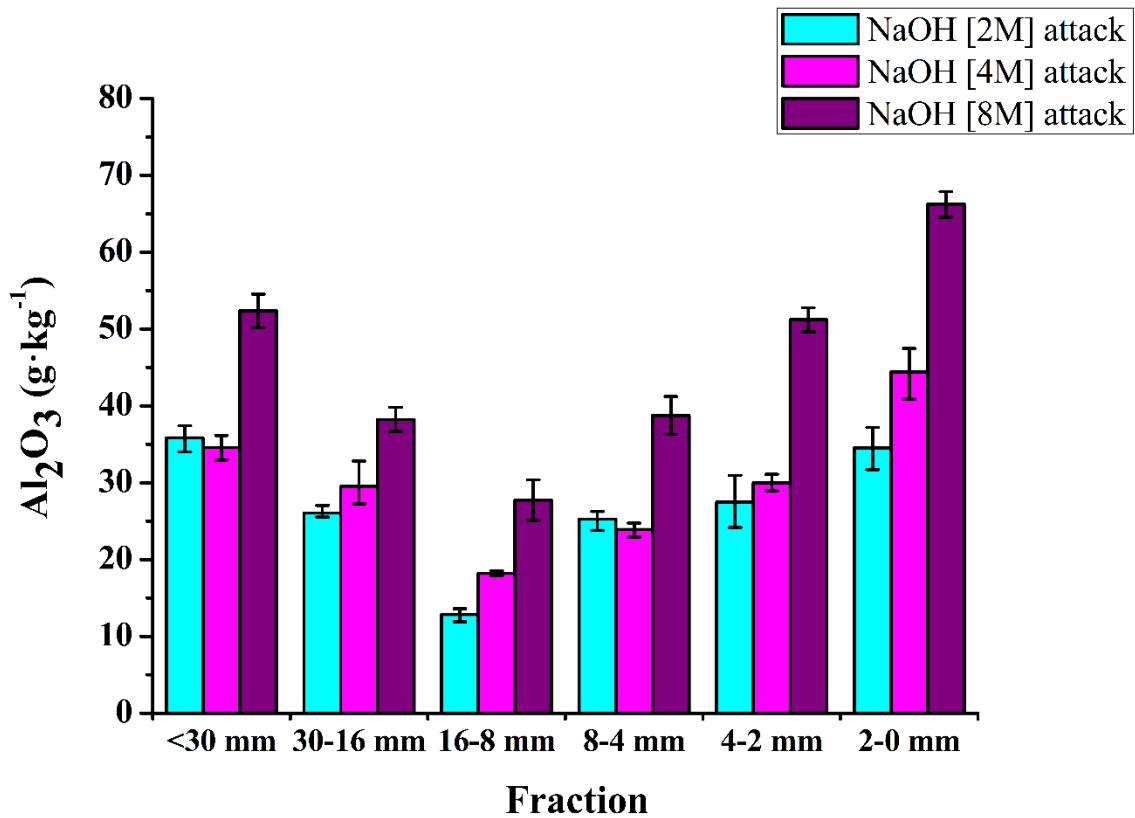
**Fig. 4. SiO<sub>2</sub> availability of WBA as a function of particle size fraction and chemical attack solution.**

Fig. 5 shows the percentage of SiO<sub>2</sub> extracted from the NaOH chemical attacks as a function of the SiO<sub>2</sub> extracted from HF chemical attack (thereby assuming that the amount extracted with the HF attack is 100% of the SiO<sub>2</sub> available in the WBA samples). The results show that it is not possible to extract the same amount of SiO<sub>2</sub> with NaOH as with HF chemical attacks, at least not under the experimental conditions of this study (particle size, NaOH concentration, agitation, and temperature).



**Fig. 5. SiO<sub>2</sub> percentage extracted from NaOH attacks as a function of HF attack.**

The Al<sub>2</sub>O<sub>3</sub> availability in Fig. 6 shows the same broad trends as in Fig. 4. Considering each particle size fraction, as the NaOH concentration increases, the Al<sub>2</sub>O<sub>3</sub> availability also increases (except for the 8-4, and 16-8 mm fractions). Regarding the trend for all the fractions as a function of the chemical attack, an inverse curve to that observed in Fig. 4 is the result, with the minimum value for the 16-8 mm fraction. Considering each fraction, as NaOH concentration increases, it is also increasing the Al<sub>2</sub>O<sub>3</sub> availability (except for the <30 and 8-4 mm fractions). The main reason for the high Al<sub>2</sub>O<sub>3</sub> availability in the finest fractions is that the Eddy current equipment only separates fractions above 10 mm, as mentioned previously. Hence, the aluminium content in fractions below 10 mm is high. The low Al<sub>2</sub>O<sub>3</sub> availability in coarse fractions is due to the high content of synthetic ceramics, which implies more Al<sub>2</sub>O<sub>3</sub> crystalline phases. The results obtained with the HF chemical attack are not shown, since this solution does not contribute to the extraction of the reactive Al<sub>2</sub>O<sub>3</sub> phases.



**Fig. 6. Al<sub>2</sub>O<sub>3</sub> availability of WBA as a function of particle size fraction and chemical attack solution.**

Considering the SiO<sub>2</sub> and Al<sub>2</sub>O<sub>3</sub> availability the SiO<sub>2</sub>/Al<sub>2</sub>O<sub>3</sub> ratio was obtained, as shown in Fig. 7. Taking into account that several authors consider the optimal SiO<sub>2</sub>/Al<sub>2</sub>O<sub>3</sub> ratio for AACs to be around 2 (Duxson et al., 2005), this matches with the <30 mm fraction (for all the NaOH chemical attacks), the 4-2 mm fraction (for NaOH 8M), the 8-4 mm fraction (for NaOH 8M), and the 2-0 mm fraction (for NaOH 4M). It should be emphasised that the other fractions need an additional source of Al<sub>2</sub>O<sub>3</sub> or SiO<sub>2</sub>, depending on their content of SiO<sub>2</sub> or Al<sub>2</sub>O<sub>3</sub>, respectively. Considering the high Al<sub>2</sub>O<sub>3</sub> availability in the finest fractions and the high SiO<sub>2</sub> availability in coarser fractions, it is expected the best results for the <30 mm fraction. This fraction presents the required ratio between the available SiO<sub>2</sub> and Al<sub>2</sub>O<sub>3</sub> content.

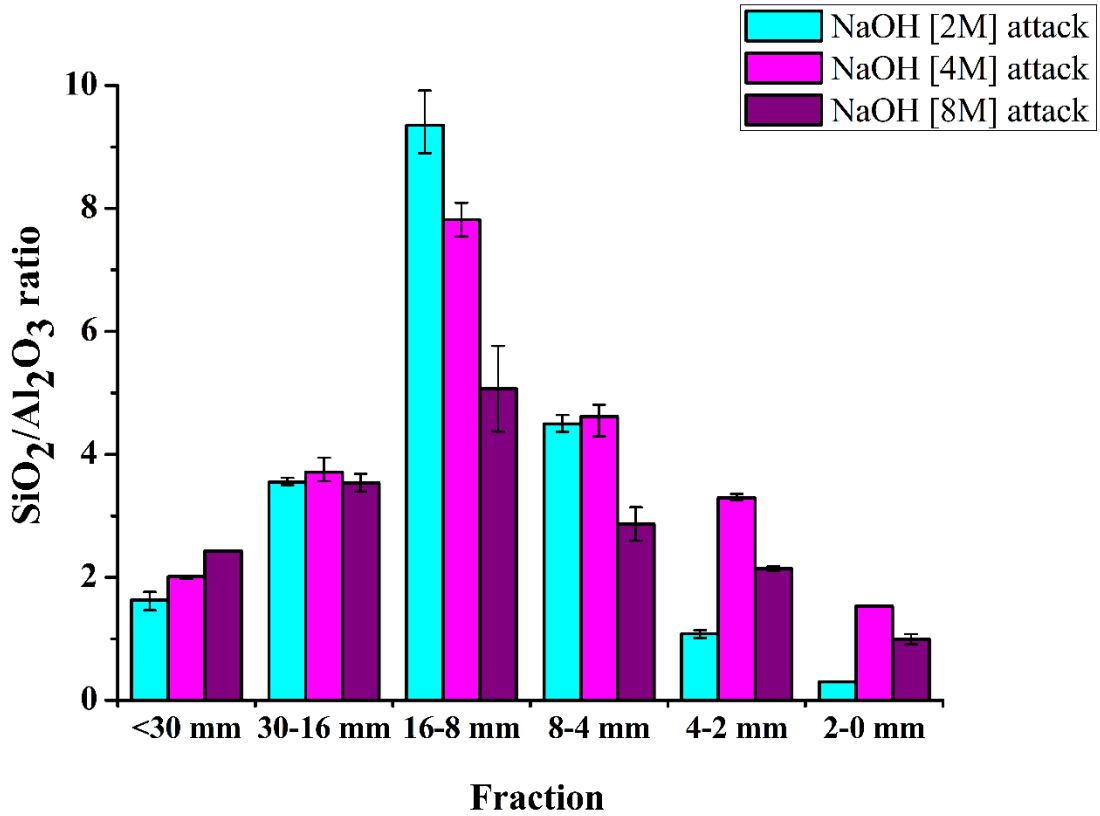


**Fig. 7. Si/Al ratio of WBA as a function of particle size fraction and chemical attack solution.**

The initial WBA FT-IR spectra for each fraction were compared to the FT-IR spectra of the attacked WBA in order to evaluate changes in its structure and composition after the chemical attacks. Fig. 8 depicts the FT-IR spectra of the initial WBA samples, according to particle size fraction. The predominant peaks observed in the spectra are typical of carbonate and silicate compounds (Criado et al., 2005). On the one hand, there is a strong band at 1429  $\text{cm}^{-1}$ , assigned to the stretching mode of carbonates, as well as sharp peaks at 875  $\text{cm}^{-1}$  and 714  $\text{cm}^{-1}$  related to the bending mode of carbonates. On the other hand, there is a broad band at 1000  $\text{cm}^{-1}$  ascribed to T-O stretching vibrations (where T=Si or Al), and a weak double peak at 780  $\text{cm}^{-1}$  associated with Si-O-Si bridging bonds in quartz ( $\text{SiO}_2$ ) (Criado et al., 2005). It can be observed a broad shoulder around 980  $\text{cm}^{-1}$  related to Si(Al)-O asymmetrical vibrations. The FT-IR results validate those of the XRF and XRD analysis, where Si and Al

1  
2  
3  
4  
5  
6  
7  
8  
9  
10  
11  
12  
13  
14  
15  
16  
17  
18  
19  
20  
21  
22  
23  
24  
25  
26  
27  
28  
29  
30  
31  
32  
33  
34  
35  
36  
37  
38  
39  
40  
41  
42  
43  
44  
45  
46  
47  
48  
49  
50  
51  
52  
53  
54  
55  
56  
57  
58  
59  
60  
61  
62  
63  
64  
65

were determined as major elements and some alumino-silicate compounds were also identified.

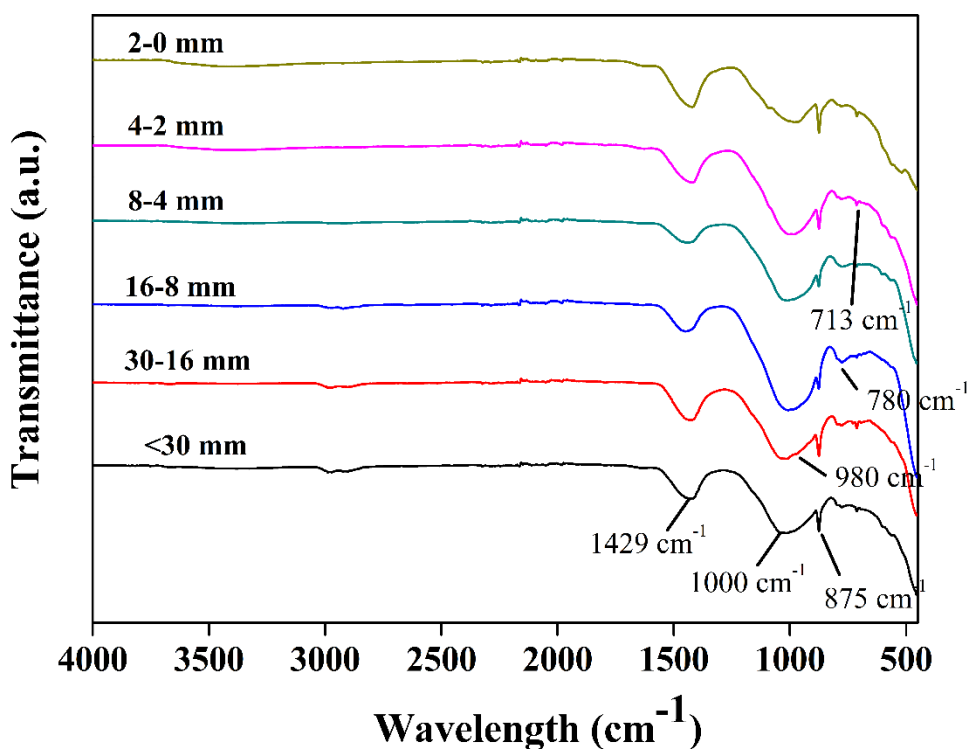
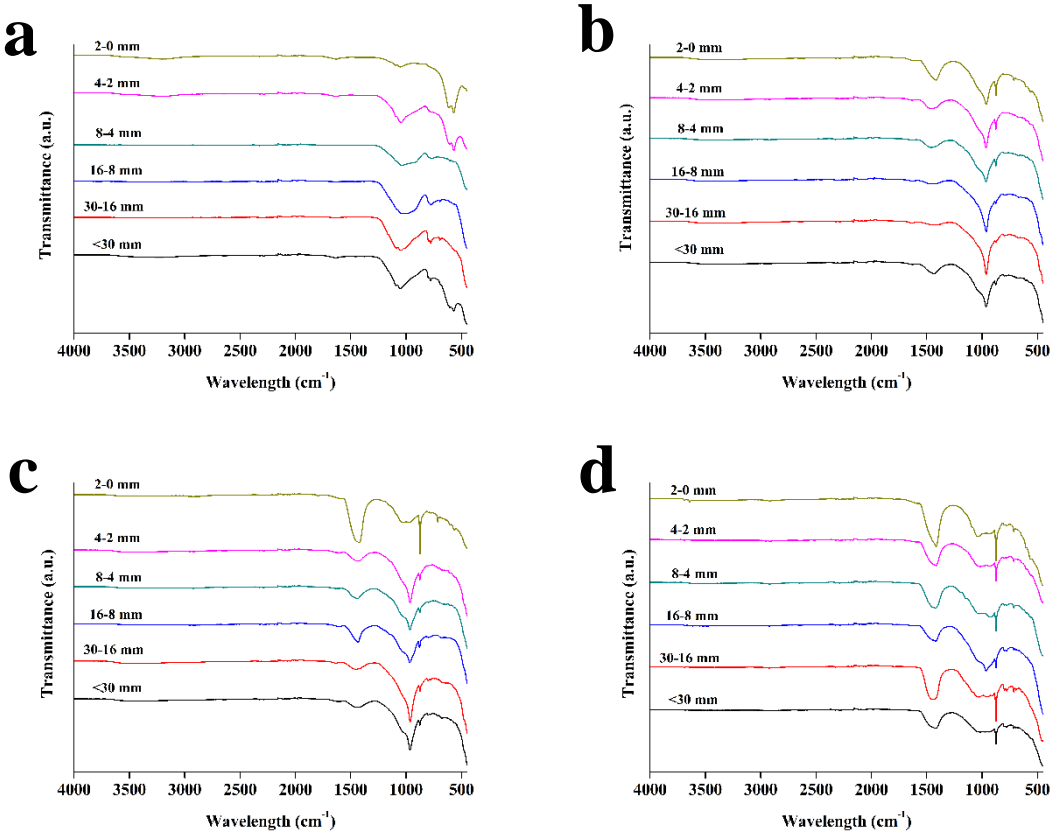


**Fig. 8. FT-IR spectrum of the particle size fractions of WBA.**

Fig. 9 shows the FT-IR spectra for all the samples as a function of the chemical attack solution, with remarkable differences between them. If the spectra of the WBA samples attacked by HF and NaOH 8M solutions are compared with the FT-IR spectrum of the initial WBA samples, a great reduction (slightly pronounced in HF) of the Si-O-Si peak can be observed. The spectra of the WBA samples attacked with NaOH 2M and NaOH 4M presents a morphological variation in the Si-O-Si peak compared with the spectrum of the initial WBA samples (a sharpening of the peak at 1000  $\text{cm}^{-1}$ ). These results agree with those obtained in the chemical attacks, where more  $\text{SiO}_2$  with the HF and NaOH 8M attacks were extracted than with the NaOH 2M and NaOH 4M attacks, due to the greater aggressiveness of the formers. It also can be observed that the initial carbonate broad band and sharp peaks

1 disappear in the HF chemical attack, in contrast with the NaOH 4M and NaOH 8M solutions,  
2 where there is an increase in the intensity of the peaks. As for NaOH 2M, both the broad band  
3 and sharp peak are slightly reduced in comparison with the initial WBA. This is all consistent  
4 and sharp peak are slightly reduced in comparison with the initial WBA. This is all consistent  
5 with the aggressiveness of the reactive solutions. When a slightly aggressive reactive solution  
6 was used (i.e. NaOH 2M), the solubility in aqueous media of some alkali-carbonates, mainly  
7 sodium and potassium carbonates was strongly affected. However, the solubility of alkaline-  
8 earth carbonates (e.g. calcium carbonate) and SiO<sub>2</sub>-based vitreous compounds was hardly  
9 affected. The aggressiveness of the reactive solution (i.e. NaOH 4M and 8M) increases the  
10 solubility of the SiO<sub>2</sub>, mainly the vitreous materials. When the solubility of alkaline-earth  
11 carbonates decreases, the relative content of the carbonates in the attacked residues increases.  
12  
13  
14  
15  
16  
17  
18  
19  
20  
21  
22  
23



24  
25  
26  
27  
28  
29  
30  
31  
32  
33  
34  
35  
36  
37  
38  
39  
40  
41  
42  
43  
44  
45  
46  
47  
48  
49  
50  
51  
52  
53 **Fig. 9. FT-IR spectra of attacked WBA samples as a function of chemical attack solution**  
54 **(a) HF (b) NaOH 2M (c) NaOH 4M (d) NaOH 8M**  
55  
56  
57  
58  
59  
60  
61  
62  
63  
64  
65

### 3.1.3. Heavy metals content

An environmental characterisation of the WBA was performed to evaluate the potential release of metal(loid)s. The study was only conducted for the worst-case scenario, corresponding to the use of the most aggressive reactive alkaline solution (i.e. NaOH 8M). The heavy metal(loid)s content ( $\text{mg}\cdot\text{kg}^{-1}$ ) is shown in Table 4. The results demonstrate that the WBA samples release more metal(loid)s with an excess of NaOH 8M. This means that the alkaline nature of NaOH 8M caused a severe activation of heavy metal(loid)s, because of the high pH value obtained, since the initial WBA is considered a non-hazardous material (Giro-Paloma et al., 2017a; Valle-zermeño et al., 2017). However, it is expected that with the formulation of AAC using WBA as precursor, most of the activated metalloids will remain encapsulated (Kupwade-Patil et al., 2014).

Table 4. Metal(loid)s content of WBA ( $\text{mg}\cdot\text{kg}^{-1}$ ) samples.

Fraction	As	Ba	Cr	Cu	Hg	Mo	Ni	Pb	Zn
<30 mm	6.06	294.58	23.39	23.87	0.05	14.84	8.04	133.30	896.00
> 16 mm	16.77	196.98	35.65	13.44	0.16	16.72	8.24	582.07	454.70
16-8 mm	12.71	385.89	10.31	18.95	0.28	16.59	8.99	477.00	325.18
8-4 mm	8.80	536.79	19.98	26.79	-	16.90	6.58	156.68	2209.05
4-2 mm	16.05	474.21	16.43	48.17	-	18.60	9.13	736.89	1710.49
2-0 mm	8.82	408.09	18.41	77.63	0.07	17.72	8.48	433.43	4187.92

## 4. Conclusions

It is necessary to find a solution to valorise the large amount of MSWI bottom ash produced around the world and especially in Europe, to promote the new environmental policies of the EU. The research reported herein demonstrates the potential of WBA for use as a precursor in the alkali-activation of cements. Physicochemical characterisation determined the composition based on aluminosilicates and the amorphous nature of WBA samples. The chemical attacks results showed that the  $\text{SiO}_2$  and  $\text{Al}_2\text{O}_3$  reactive phases are available in each particle size fraction of the WBA. The calculated Si/Al ratio of each WBA sample suggests the possibility of formulating AACs using WBA as sole precursor, or mixed with others, in order to adjust the Si/Al ratio to around 2. The environmental characterisation of WBA

1 samples showed a high activation of heavy metal(loid)s, due to the redissolution of the pH-  
2 dependent metal(loid)s in high pH media, generated by the alkaline reactive solutions.  
3

4 The investigation future line will be based on the formulation of AACs using WBA as  
5 only precursor. The main goal must be valorising the maximum amount of WBA (using >30  
6 mm sample or mixing some fractions) without affecting to the AACs environmental  
7 properties. It will certainly be necessary to study the release of heavy metals and metal(loid)s  
8 from new AACs developed using WBA as a precursor to elucidate if it means a limitation on  
9 the final environmental properties of the materials. It is expected that to obtain AACs, there  
10 will be less release due to the encapsulation of metal(loid)s in the binder matrix and a  
11 decrease of the permeability of leaching solutions. Otherwise, WBA will be mixed with other  
12 more noble precursors in order to dilute the concentration of the heavy metal(loid)s content.  
13  
14  
15  
16  
17  
18  
19  
20  
21  
22  
23  
24  
25

## 26 **Acknowledgements**

27 The work is partially funded by the Spanish Government (BIA2017-83912-C2-1-R). The  
28 authors would like to thank the Catalan Government for the quality accreditation given to  
29 their research groups DIOPMA (2017 SGR 118). The authors also want to thank SIRUSA and  
30 VECSA for supplying MWI Bottom Ash. Mr. Alex Maldonado-Alameda is grateful to the  
31 Government of Catalonia for the research Grant (FI-DGR 2017).  
32  
33  
34  
35  
36  
37  
38  
39  
40  
41

## 42 **References**

43 Aljerf, L., 2015. Effect of Thermal-cured Hydraulic Cement Admixtures on the Mechanical  
44 Properties of Concrete. *Interceram - Int. Ceram. Rev.* 64, 346–356.

45 <https://doi.org/10.1007/BF03401142>

46 Alonso, S., Vázquez, T., Puertas, F., Martínez-Ramírez, S., 2000. Alkali-activated fly ash /  
47 slag cement Strength behaviour and hydration products. *Cem. Concr. Res.* 30, 1625–  
48

49 1632. [https://doi.org/10.1016/S0008-8846\(00\)00298-2](https://doi.org/10.1016/S0008-8846(00)00298-2)

50 Arm, M., 2003. Mechanical properties of residues as unbound road materials - experimental  
51  
52  
53  
54  
55  
56  
57  
58  
59  
60  
61  
62  
63  
64  
65

tests on MSWI bottom ash, crushed concrete and blast furnace slag.

1  
2 Bakharev, T., 2005. Resistance of geopolymer materials to acid attack. *Cem. Concr. Res.* 35,  
3  
4 658–670. <https://doi.org/10.1016/j.cemconres.2004.06.005>  
5  
6

7 Bernal, S.A., Rodríguez, E.D., Kirchheim, A.P., Provis, J.L., 2016. Management and  
8  
9 valorisation of wastes through use in producing alkali-activated cement materials. *J.*  
10  
11 *Chem. Technol. Biotechnol.* 91, 2365–2388. <https://doi.org/10.1002/jctb.4927>  
12  
13

14 CEWEP, 2016. Bottom ash fact sheet.  
15

16 Chen, I.A., 2009. Synthesis of Portland Cement and Calcium Sulfoaluminate-Belite Cement  
17  
18 for Sustainable Development and Performance. *PCA R&D Ser. No. SN3130* 1–216.  
19  
20

21 Cheng, H., Hu, Y., 2010. Municipal solid waste (MSW) as a renewable source of energy:  
22  
23 Current and future practices in China. *Bioresour. Technol.* 101, 3816–3824.  
24  
25  
26 <https://doi.org/10.1016/j.biortech.2010.01.040>  
27  
28

29 Chimenos, J., Segarra, M., Fernández, M., Espiell, F., 1999. Characterization of the bottom  
30  
31 ash in municipal solid waste incinerator. *J. Hazard. Mater.* 64, 211–222.  
32  
33  
34 [https://doi.org/10.1016/S0304-3894\(98\)00246-5](https://doi.org/10.1016/S0304-3894(98)00246-5)  
35

36 Chimenos, J.M., Fernández, A.I., Miralles, L., Segarra, M., Espiell, F., 2003. Short-term  
37  
38 natural weathering of MSWI bottom ash as a function of particle size. *Waste Manag.* 23,  
39  
40 887–895. [https://doi.org/10.1016/S0956-053X\(03\)00074-6](https://doi.org/10.1016/S0956-053X(03)00074-6)  
41  
42

43 Chimenos, J.M., Fernandez, A.I., Nadal, R., Espiell, F., 2000. Short term natural weathering  
44  
45 of MSWI bottom ash. *J. Hazard. Mater.* B79 79, 287–299.  
46  
47

48 Cioffi, R., Colangelo, F., Montagnaro, F., Santoro, L., 2011. Manufacture of artificial  
49  
50 aggregate using MSWI bottom ash. *Waste Manag.* 31, 281–288.  
51  
52  
53 <https://doi.org/10.1016/j.wasman.2010.05.020>  
54  
55

56 Criado, M., Palomo, A., Fernández-Jiménez, A., 2005. Alkali activation of fly ashes. Part 1:  
57  
58 Effect of curing conditions on the carbonation of the reaction products. *Fuel* 84, 2048–  
59  
60

2054. <https://doi.org/10.1016/j.fuel.2005.03.030>

1  
2 Duxson, P., Fernández-Jiménez, A., Provis, J.L., Lukey, G.C., Palomo, A., Van Deventer,  
3  
4 J.S.J., 2007. Geopolymer technology: The current state of the art. *J. Mater. Sci.* 42,  
5  
6 2917–2933. <https://doi.org/10.1007/s10853-006-0637-z>

7  
8  
9 Duxson, P., Provis, J.L., Lukey, G.C., Mallicoat, S.W., Kriven, W.M., Van Deventer, J.S.J.,  
10  
11 2005. Understanding the relationship between geopolymer composition, microstructure  
12  
13 and mechanical properties. *Colloids Surfaces A Physicochem. Eng. Asp.* 269, 47–58.  
14  
15  
16 <https://doi.org/10.1016/j.colsurfa.2005.06.060>

17  
18  
19 European Commission, 2015. Directive of the European Parliament and of the Council -  
20  
21 amending Directive 94/62/EC on packaging and packaging waste.  
22  
23  
24 <https://doi.org/10.1007/s13398-014-0173-7.2>

25  
26 European Commission, 2017. Report from the commission to the european parliament, the  
27  
28 council, the european economic and social committee and the committee of the regions.  
29  
30  
31 Off. J. Eur. Union COM(2017), 1–14.

32  
33  
34 European Parliament and Council, 2008. Directive 2008/98/EC of the European Parliament  
35  
36 and of the Council of 19 November 2008 on waste and repealing certain directives. Off.  
37  
38  
39 J. Eur. Union 3–30. <https://doi.org/2008/98/EC.; 32008L0098>

40  
41 Ginés, O., Chimenos, J.M., Vizcarro, A., Formosa, J., Rosell, J.R., 2009. Combined use of  
42  
43 MSWI bottom ash and fly ash as aggregate in concrete formulation: Environmental and  
44  
45 mechanical considerations. *J. Hazard. Mater.* 169, 643–650.  
46  
47  
48 <https://doi.org/10.1016/j.jhazmat.2009.03.141>

49  
50  
51 Giro-Paloma, J., Maldonado-Alameda, A., Formosa, J., Barbieri, L., Chimenos, J.M.,  
52  
53 Lancellotti, I., 2017a. Geopolymers based on the valorization of Municipal Solid Waste  
54  
55 Incineration residues, in: *IOP Conference Series: Materials Science and Engineering*.  
56  
57  
58 <https://doi.org/10.1088/1757-899X/251/1/012125>

- 1  
2  
3  
4  
5  
6  
7  
8  
9  
10  
11  
12  
13  
14  
15  
16  
17  
18  
19  
20  
21  
22  
23  
24  
25  
26  
27  
28  
29  
30  
31  
32  
33  
34  
35  
36  
37  
38  
39  
40  
41  
42  
43  
44  
45  
46  
47  
48  
49  
50  
51  
52  
53  
54  
55  
56  
57  
58  
59  
60  
61  
62  
63  
64  
65
- Giro-Paloma, J., Ribas-Manero, V., Maldonado-Alameda, A., Formosa, J., Chimenos, J.M., 2017b. Use of municipal solid waste incineration bottom ash and crop by-product for producing lightweight aggregate, in: IOP Conference Series: Materials Science and Engineering. <https://doi.org/10.1088/1757-899X/251/1/012126>
- Hjelmar, O., Holm, J., Crillesen, K., 2007. Utilisation of MSWI bottom ash as sub-base in road construction: First results from a large-scale test site. *J. Hazard. Mater.* 139, 471–480. <https://doi.org/10.1016/j.jhazmat.2006.02.059>
- Jansen, D., Stabler, C., Goetz-Neunhoeffler, F., Dittrich, S., Neubauer, J., 2011. Does Ordinary Portland Cement contain amorphous phase? A quantitative study using an external standard method. *Powder Diffr.* 26, 31–38. <https://doi.org/10.1154/1.3549186>
- Johansson, I., Bavel, B. Van, 2003. Polycyclic aromatic hydrocarbons in weathered bottom ash from incineration of municipal solid waste. *Chemosphere* 53, 123–128. [https://doi.org/10.1016/S0045-6535\(03\)00299-6](https://doi.org/10.1016/S0045-6535(03)00299-6)
- Komnitsas, K.A., 2011. Potential of geopolymer technology towards green buildings and sustainable cities. *Procedia Eng.* 21, 1023–1032. <https://doi.org/10.1016/j.proeng.2011.11.2108>
- Kupwade-Patil, K., Allouche, E.N., Islam, R., Gunasekaran, A., 2014. Encapsulation of solid waste incinerator ash in geopolymer concretes and its applications. *ACI Mater. J.* 111, 691–700. <https://doi.org/10.14359/51686834>
- Lancellotti, I., Ponzoni, C., Bignozzi, M.C., Barbieri, L., Leonelli, C., 2014. Incinerator bottom ash and ladle slag for geopolymers preparation. *Waste and Biomass Valorization* 5, 393–401. <https://doi.org/10.1007/s12649-014-9299-2>
- Magnusson, Y., 2005. Environmental Systems Analysis for utilisation of bottom ash in ground constructions. *Trita-KET-IM*.
- McLellan, B.C., Williams, R.P., Lay, J., Van Riessen, A., Corder, G.D., 2011. Costs and

- 1 carbon emissions for geopolymer pastes in comparison to ordinary portland cement. J.  
2 Clean. Prod. 19, 1080–1090. <https://doi.org/10.1016/j.jclepro.2011.02.010>  
3  
4 Murri, A.N., Rickard, W.D.A., Bignozzi, M.C., Riessen, A. Van, 2013. High temperature  
5 behaviour of ambient cured alkali-activated materials based on ladle slag. Cem. Concr.  
6 Res. 43, 51–61. <https://doi.org/10.1016/j.cemconres.2012.09.011>  
7  
8 Pecqueur, G., Crignon, C., Que, B., 2001. Behaviour of cement-treated MSWI bottom ash 21,  
9 229–233.  
10  
11 Pérez-Martínez, S., Giro-paloma, J., Maldonado-alameda, A., Formosa, J., Queralt, I., 2019.  
12 Characterisation and partition of valuable metals from WEEE in weathered municipal  
13 solid waste incineration bottom ash , with a view to recovering 218, 61–68.  
14  
15 <https://doi.org/10.1016/j.jclepro.2019.01.313>  
16  
17 Phair, J.W., 2006. Green chemistry for sustainable cement production and use. Green Chem.  
18 8, 763–780. <https://doi.org/10.1039/b603997a>  
19  
20 Roy, D.M., 1999. Alkali-activated cements: Opportunities and challenges. Cem. Concr. Res.  
21 29, 249–254. [https://doi.org/10.1016/S0008-8846\(98\)00093-3](https://doi.org/10.1016/S0008-8846(98)00093-3)  
22  
23 Ruiz-Santaquiteria, C., Fernández-Jiménez, a, Palomo, a, 2011. Quantitative determination  
24 of reactive SiO<sub>2</sub> and Al<sub>2</sub>O<sub>3</sub> in aluminosilicate materials. 13th Int. Congr. Chem. Cem.  
25 1–7.  
26  
27 Shim, Y., Kim, Y., Kong, S., Rhee, S., Lee, W., 2003. The adsorption characteristics of heavy  
28 metals by various particle sizes of MSWI bottom ash. Waste Manag. 23, 851–857.  
29  
30 [https://doi.org/10.1016/S0956-053X\(02\)00163-0](https://doi.org/10.1016/S0956-053X(02)00163-0)  
31  
32 Silva, R. V., de Brito, J., Lynn, C.J., Dhir, R.K., 2017. Use of municipal solid waste  
33 incineration bottom ashes in alkali-activated materials, ceramics and granular  
34 applications: A review. Waste Manag. 68, 207–220.  
35  
36 <https://doi.org/10.1016/j.wasman.2017.06.043>  
37  
38  
39  
40  
41  
42  
43  
44  
45  
46  
47  
48  
49  
50  
51  
52  
53  
54  
55  
56  
57  
58  
59  
60  
61  
62  
63  
64  
65

- 1  
2  
3  
4  
5  
6  
7  
8  
9  
10  
11  
12  
13  
14  
15  
16  
17  
18  
19  
20  
21  
22  
23  
24  
25  
26  
27  
28  
29  
30  
31  
32  
33  
34  
35  
36  
37  
38  
39  
40  
41  
42  
43  
44  
45  
46  
47  
48  
49  
50  
51  
52  
53  
54  
55  
56  
57  
58  
59  
60  
61  
62  
63  
64  
65
- Singh, B., G., I., Gupta, M., Buattacharyya, S.K., 2015. Geopolymer Concrete : A Review of some recent developments. *Constr. Build. Mater.* 85, 78–90.
- Snellings, R., Salze, A., Scrivener, K.L., 2014. Use of X-ray diffraction to quantify amorphous supplementary cementitious materials in anhydrous and hydrated blended cements. *Cem. Concr. Res.* 64, 89–98. <https://doi.org/10.1016/j.cemconres.2014.06.011>
- Toraldo, E., Saponaro, S., Careghini, A., Mariani, E., 2013. Use of stabilized bottom ash for bound layers of road pavements. *J. Environ. Manage.* 121. <https://doi.org/10.1016/j.jenvman.2013.02.037>
- Valle-zermeño, R., Formosa, J., Chimenos, J.M., 2017. Material characterization of the MSWI bottom ash as a function of particle size . Effects of glass recycling over time. *Sci. Total Environ.* 581–582, 897–905. <https://doi.org/10.1016/j.scitotenv.2017.01.047>
- Van Deventer, J.S.J., Provis, J.L., Duxson, P., 2012. Technical and commercial progress in the adoption of geopolymer cement. *Miner. Eng.* 29, 89–104. <https://doi.org/10.1016/j.mineng.2011.09.009>
- Wei, Y., Shimaoka, T., Saffarzadeh, A., Takahashi, F., 2011. Mineralogical characterization of municipal solid waste incineration bottom ash with an emphasis on heavy metal-bearing phases. *J. Hazard. Mater.* 187, 534–543. <https://doi.org/10.1016/j.jhazmat.2011.01.070>
- Yao, W.J., Fan, L., Liu, G.Y., 2018. Properties of Alkali-Activated Waste Glass-Cement Cementitious Materials. *Mater. Sci. Forum* 926, 134–139. <https://doi.org/10.4028/www.scientific.net/MSF.926.134>
- Zhang, H., Shimaoka, T., 2013. Formation of Humic Substances in Weathered MSWI Bottom Ash. *Sci. World J.* 2013.